View metadata, citation and similar papers at core.ac.uk
brought to you by CORE
provided by Scholarship@Western

RESILIENT INFRASTRUCTURE
June 1–4, 2016
RESILIENT INFRASTRUCTURE LONDON 2016

FLEXURAL BEHAVIOUR AND BOND-DEPENDENT COEFFICIENT OF BASALT FRP BARS IN CONCRETE BEAMS

Fareed Elgabbas
PhD Candidate, Université de Sherbrooke, Canada

Ehab Ahmed
Postdoctoral Fellow, Université de Sherbrooke, Canada

Brahim Benmokrane
Professor, Université de Sherbrooke, Canada
NSERC Research Chair in FRP Reinforcement for Concrete Infrastructure
Tier-1 Canada Research Chair in Advanced Composite Materials for Civil Structures

ABSTRACT

This paper presents an experimental study aimed at determining the bond-dependent coefficient (k_b) and investigating the flexural performance of concrete beams reinforced with ribbed basalt fiber-reinforced polymer (BFRP) bars. The performance of the BFRP-RC concrete beams is compared against that of GFRP-RC ones. A total of five concrete beams measured 200 mm wide × 300 mm deep × 3100 mm long were constructed and tested in four-point bending over a clear span of 2700 mm. The main variables were reinforcement type (BFRP, GFRP, and steel bars as reference) and reinforcement ratio. The test results showed that the average k_b was 0.85 for the ribbed BFRP bars. The k_b value of ribbed BFRP bars was lower than 1.0 recommended by the Canadian Highway Bridge Design Code, CHBDC (CSA S6-14).

Keywords: Fiber-Reinforced Polymer, Basalt, Glass, Flexure, Deflection, Crack width, k_b.

1. INTRODUCTION

Deterioration of reinforced concrete (RC) structures due to corrosion of steel reinforcement is a major concern. The use of de-icing materials and the dominance of aggressive environment are the origin of the corrosion problem. This fact provides an indication of the big financial burden associated with the replacement of the deteriorated structures with the new materials, which has been estimated to be twice the original construction cost (Boyle and Karbhari, 1994). Therefore, finding new materials such as fiber-reinforced-polymer (FRP) that can fulfill the above requirements is a must. Moreover, the advances in the FRP technology have spurred interest in introducing new fibers, such as basalt, in addition to the commonly used glass, carbon, and aramid. The recent basalt FRP (BFRP) has the potential to offer an efficient and cost-effective solutions when implemented in concrete structure.

Furthermore, the available design codes and guides such as ACI 440.1R (2015), CSA S6 (2014) and CSA S806 (2012) allow the use of glass, carbon, and aramid FRP bars as primary reinforcement. However, they are not providing recommendations for the use of BFRP bars since fundamental studies and relevant applications are still limited. Therefore, investigations are needed to characterize and understand the behavior of BFRP bars in concrete members.

This study aims at determining the bond-dependent coefficient (k_b) and investigating the flexural performance of concrete beams reinforced with ribbed basalt FRP (BFRP) bars. To compare the behaviour against the commonly used GFRP reinforcing bars, the investigation was extended to include two beams reinforced with sand-coated GFRP bars. A steel-reinforced concrete beam was also included as reference.

2. EXPERIMENTAL PROGRAM

2.1 Material Properties

Reinforcing Bars: Basalt and glass FRP bars of size #5 (16 mm) were used in this study. The BFRP and GFRP bars were fabricated using pultrusion in a vinylesters resin with fiber contents of 80% and 82%, respectively. The BFRP bars have a ribbed surface, while the GFRP bars have a sand-coated surface. The tensile properties of the FRP bars were determined by testing five representative specimens of each type according to ASTM D7025 (2011). Moreover, 10M deformed steel bars were used for the reference beam. Table 1 summarizes the mechanical properties of the reinforcing bars. Figure 1 shows the surface configuration of the BFRP, GFRP and steel bars.

Table 1: Tensile properties and surface configurations of the reinforcing bars

RFT Type/Size	d_b (mm)	A_f (mm²)	E_f (GPa)	f_{fu} (MPa)	ε_{fu} (%)	Surface configuration
BFRP/No. 5	16.0	199	64.8	1724	2.67	Ribbed
GFRP/No. 5	16.0	199	62.6	1286	2.05	Sand-coated
Steel/10M	11.3	100	200.0	f_y^* = 450	ε_y^* = 0.2	Deformed

** f_y and ε_y are the yield strength and strain of the steel bars, respectively.

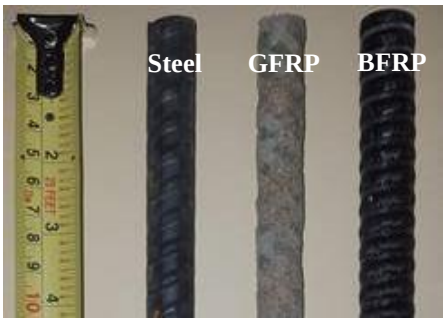

Figure 1: Reinforcing bars

Concrete: The concrete beams were constructed using ready-mixed concrete of normal-weight with a target 28-days compressive strength of 40 MPa. The maximum size of the coarse aggregates was 20 mm. The concrete compressive strength of each batch was determined by testing three 150×300 mm cylinders while the tensile strength was determined from split-cylinder testing. Table 2 provides the concrete compressive and tensile strengths.

2.2 Test Specimens

A total of five RC beams were constructed and tested up to failure. The tested beams measured 3100 mm long, 200 mm wide, and 300 mm deep, as shown in Figure 2. The beams had a 200 mm overhang length beyond the supports on each side as anchorage length to avoid bond failure. The beam specimens were provided with 10M stirrups each 100 mm in the shear spans to avoid shear failure. Each specimen was reinforced longitudinally with 2 10M steel bars as top reinforcement and different reinforcement ratios and types at the bottom. The clear concrete cover was 38 mm CSA S806 (2012). Table 2 presents the reinforcement details of each beam. Figure 2 also shows the typical reinforcement details of the beam specimens, while Figure 3 shows the fabrication of the tested specimens.

Table 2: Test matrix, reinforcement details and mechanical properties of the tested beams

Code*	f'_c (MPa)	f_t (MPa)	Bot. RFT	ρ (%)	ρ/ρ_b		$E\times A$ (kN)
					ACI 440-06	CSA S806-12	
B-2#16	50.8±1.7	4.2±0.3	2#16mm	0.79	4.577	3.545	26068
B-3#16			3#16mm	1.19	6.865	5.238	39102
G-2#16			2#16mm	0.79	2.685	2.112	24915
G-3#16			3#16mm	1.19	4.028	3.168	37372
S-2#10M	44.7±2.0	4.3±0.3	2#10M	0.39	0.103	0.096	40000

* Reinforcement type (B: BFRP; G: GFRP; S: Steel) followed by the number of bars and bar size.

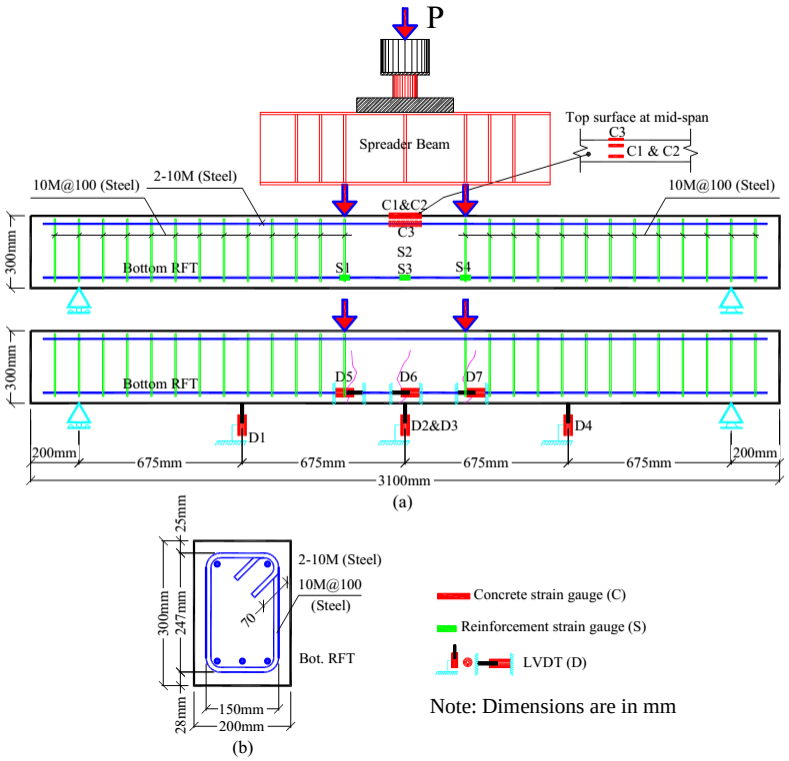

Figure 2: Schematic drawing for concrete dimensions, reinforcement details, typical location of instrumentation and test setup: (a) Elevation; (b) Cross- sections

Figure 3: Fabrication of the beam specimens

2.3 Instrumentation and Test Setup

Electrical-resistance strain gauges were used to measure the tensile strains in the bottom reinforcing bars and the compressive strains in the concrete beams at the desired locations. Four electrical strain gauges (6 mm) were glued on the longitudinal reinforcing bars in the middle of the beam and under the loading points [S1 to S4]. In addition, two electrical strain gauges (60 mm) were glued on the top surface of the concrete beams at mid-span to measure the concrete compressive strains [C1 and C2]. The deflection along the beam's span was monitored using four LVDTs, labeled D1 to D4. Crack propagation was also monitored during testing until failure, and the crack widths of the first three flexural cracks were monitored with three horizontal LVDTs [D5 to D7]. To facilitate crack monitoring, the beams were painted white prior to testing. In addition, an automatic data-acquisition system connected to a computer was used to monitor loading, deflections, and strains in the concrete and reinforcement. Figure 3 shows typical location of instrumentations.

The specimens were tested in four-point bending over a simply-supported clear span of 2700 mm. The load was applied using a 500 kN closed-loop MTS actuator with a stroke-controlled rate of 1.2 mm/min. The loading was stopped when the first three flexural cracks appeared and the initial crack widths were measured manually using a handheld 50X microscope. Thereafter, the LVDTs were installed to continuously monitor the crack widths with the load increase. Figure 4 shows an overview of the test setup during a beam test.

Figure 4: Overview of the test setup

3. TEST RESULTS AND DISCUSSION

3.1 Cracking Moment and Pattern

The crack propagation in the tested beams is shown in Figure 5. The first cracks always appeared in the constant-moment region of the beams, starting from the beam bottom surface and extending vertically toward the compression zone. As the load increased, the cracks extended further away from the constant-moment region towards the supports. Cracks outside the constant-moment region were affected by a combination of flexural and shear stresses, so the cracks tended to gain a horizontal component. As expected, increasing the reinforcement ratio, while keeping the mechanical properties unchanged, helped enhance the cracking performance.

All beams behaved similarly until first cracking. Their cracking loads and pre-cracked stiffness were essentially the same regardless of reinforcement ratio. Table 3 provides the cracking moments (M_{cr}) of all tested beams. The reported cracking moment, excluding the self-weight of the beams, ranged from 7.62 to 9.06 kN.m with an average of 8.07 kN.m. The cracking moments were predicted using Eq. (1).

[1] $M_{cr}=(f_r \times I_g)/y_t$,where f_r is the modulus of rupture of concrete

Table 3 compares the experimental and predicted values of the cracking moments, M_{cr}. The cracking moment was generally 38% and 36% lower than those predicted with ACI 440.1R (2015) and CSA S806 (2012), respectively. CSA S806 (2012) yielded slightly better predictions of cracking moments than ACI 440.1R (2015) because of the former's smaller modulus of rupture. Similar observations were reported for the cracking moments of GFRP-RC beams (El-Nemr et al. 2013) where the predicted cracking moments were higher than the measured cracking moments for normal- and high-strength concrete. It is worth mentioning that FRP-RC members may crack over time as additional stresses developed from shrinkage, temperature effect (Bischoff 2001) and the freezing and melting of water inside the concrete, causing hair cracks and therefore reducing the cracking load. The cracks resulting from shrinkage, however, did not significantly affect crack-width prediction (Bischoff 2001).

Table 3: Cracking and ultimate moments and mode of failure

Beam	Experimental (kN.m)			ACI (2015)		CSA (2012)		k_b	Aver. k_b
	M_{cr}	M_n	M.O.F*	$\frac{M_{cr,Exp.}}{M_{cr,Pre.}}$	$\frac{M_{n,Exp.}}{M_{n,Pre.}}$	$\frac{M_{cr,Exp.}}{M_{cr,Pre.}}$	$\frac{M_{n,Exp.}}{M_{n,Pre.}}$		
B-2#16	7.62	69.83	CC	0.57	0.97	0.59	0.86	0.73	0.85
B-3#16	7.67	89.77	CC	0.58	1.06	0.60	0.95	0.96	
G-2#16	7.59	82.23	CC	0.57	1.16	0.59	1.03	N/A	
G-3#16	9.06	87.04	CC	0.68	1.04	0.71	0.93		
S-2#10M	8.40	23.57	SY+CC	0.68	--	0.70	--	--	
Average ± S.D.	8.07 ±0.65	--	--	0.62 ±0.06	1.06 ±0.08	0.64 ±0.06	0.94 ±0.07	0.85 ±0.24	

* CC: Crushing of concrete; SY+CC: Steel yielding followed by concrete crushing.

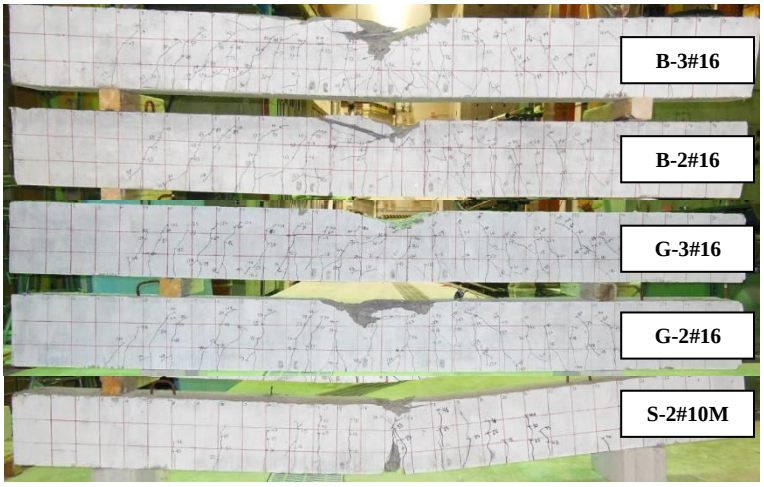

Figure 5: Crack pattern at failure of tested beams

3.2 Flexural Capacity and Mode of Failure

Table 3 presents the flexural capacity (M_n) and mode of failure of the tested beams. The tested FRP-RC beams failed by concrete crushing, as designed for over-reinforced section. While the steel-RC beam was failed due to steel yielded followed by concrete crushing as designed for under-reinforced section. Moreover, Table 3 shows that the increasing the reinforcement ratio (ρ) or axial flexure stiffness ($E\times A$) by 50% led to an increase in the ultimate capacity by 28.6% and 5.9% for the BFRP- and GFRP-RC beams, respectively.

On the other hand, B-2#10M failed at 23.57 kN.m, which is lower than the capacities of B-3#16mm and G-2#16mm with similar axial stiffness. The average flexural capacity of the FRP-RC beams was 3.75 times greater than that of the steel-RC beam with similar axial stiffness. This was attributed to the higher tensile strength and strain capacity of the BFRP bars compared to the yield stress and strain of the steel bars.

The ultimate capacity of the test specimens was predicted using the strain compatibility approach in ACI 440.1R (2015) and CSA S806 (2012) and compared to the measured values. Table 3 shows the experimental-to-predicted ultimate capacity of the tested beams. Generally, both the ACI 440.1R (2015) and CSA S806 (2012) prediction equations under- and over-estimated the flexure capacity of BFRP-RC beams. The average experimental-to-predicted ultimate capacities were 1.06±0.08 and 0.94±0.07 for ACI 440.1R (2015) and CSA S806 (2012), respectively. Moreover, the difference between ACI 440.1R (2015) and CSA S806 (2012) was related to the β_1 factor and the assumed strain at ultimate which is 0.003 for ACI 440.1R (2015) and 0.0035 for CSA S806 (2012).

3.3 Reinforcement and Concrete Strains

Figure 6 shows the measured mid-span tensile strains in the reinforcing bars as well as the mid-span concrete strains versus the applied moment for the tested beams. The figure shows similar pre-cracking responses of BFRP-, GFRP- and steel-RC beams, as well as significant post-cracking increases in the tensile and compression strains until failure, as a result of reduced post-cracking stiffness of all beams. Moreover, the plotted data shows that before and after cracking, beams reinforced with BFRP and GFRP bars exhibited tensile and compression strains vary linearly with load up to failure while beam reinforced with steel bars exhibited bi-linear response with a yield plateau in the final phase of loading after strain of 2500 μs. Figure 6 also shows that, at the same load level, beams with similar axial stiffness (B-2#16 and G-2#16) (B-3#16, G-3#16 and S-2#10M) have approximately similar tensile and compression strains regardless the reinforcement type or surface configuration. Increasing the reinforcement ratio led to decreasing the strains in the reinforcing bars and in concrete and decreasing the sharp changes of tensile strains at first crack. This is due to sudden reduction of inertia after cracking which is affected by the reinforcement ratio. Steel-RC beams, however, did not experience this jump due to energy absorption of steel bars. In addition, the measured strains in the FRP reinforcing bars are used to evaluate the bond-dependent coefficient (k_b). Table 3 shows the tensile and compressive strains of the reinforcing bars and concrete at service load (30% of the nominal capacity, 0.3M_n, as reported by Mota et al. 2006, Bischoff et al. 2009, and El-Nemr et al. 2013). ISIS (2007) recommended a value of 2000 με as a limit for the strain in FRP bars under service load. As shown in Table 3, the strains in the

BFRP and GFRP bars at 0.30M_n were high and ranged from 3907 to 5083 με. El-Nemr et al. (2013) reported high stain values up to 5349 με and Kassem et al. (2011) also reported strain values as high as 4119 με in GFRP bars at 0.3M_n.

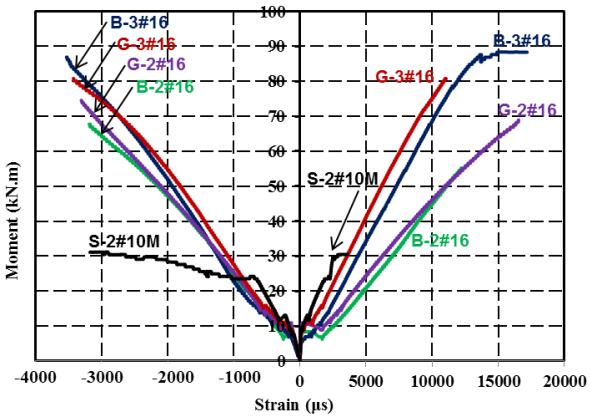

Figure 6: Moment-strain relationships for concrete and reinforcement

3.4 Deflection Behaviour

Figure 7 shows the applied moment versus the average mid-span deflection for the tested beams. The figure provides typical bi-linear moment-deflection relationships for the tested FRP-RC beams and tri-linear with a yielding plateau for the tested steel-RC beams. The beams' responses are nearly similar pre-cracking stiffness and cracking loads, due to the negligible effect of the reinforcement ratio and modulus on the gross moment of inertia of the beams. Unlike the pre-cracking stage, all tested beams exhibited lower post-cracking stiffness until failure. It is clear that the reinforcement ratio shows significant influence on the beams' post-cracking responses until the failure. As expected, larger deformations were noted for lower reinforcement ratios and axial stiffness. In addition, providing approximately the same axial stiffness ($E \times A$) for beam B-3#16, G-3#16 and S-2#10M; resulted in similar moment-deflection relationships up to yielding of steel bars. The moment-deflection relationships were not affected by the type or surface configuration of the reinforced bars when the same axial stiffness was provided and no slippage was occurred.

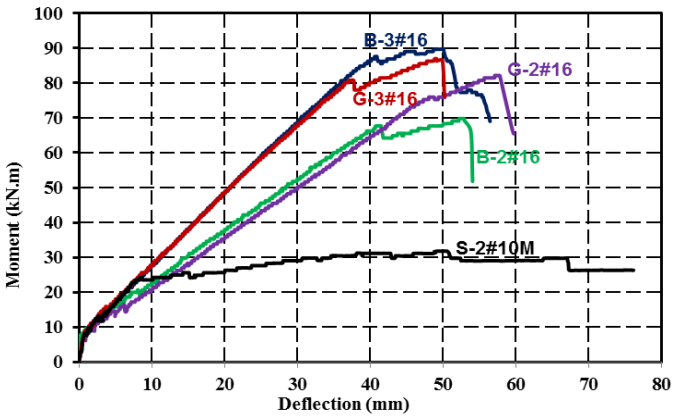

Figure 7: Moment-average mid-span deflection relationships

3.5 Crack Width and Bond-Dependent Coefficient (k_b) Prediction

The test results were used to assess the bond-dependent coefficient values (k_b) of ribbed BFRP bars. The k_b was calculated from Eq. (2) (CSA S806 2012). The calculations were based on the first three cracks in each beam. The k_b was calculated from each beam at 0.3M_n (assumed service load) of the tested specimens and is presented in Table 3.

The average k_b value was 0.85 for ribbed BFRP bars which is lower than the recommended value of 1.0 provided by CSA S6 (2014), which means the BFRP bars exhibited better bond and lower crack widths than the expected.

[2] $$w_{cr} = 2\frac{f_f}{E_f}\frac{h_2}{h_1}k_b\sqrt{d_c^{\,2}+(s/2)^2}$$

where w_{cr} is the maximum crack width (mm), E_f is the modulus of elasticity of FRP bar (MPa), f_f is the stress in FRP reinforcement in tension (MPa), k_b is the bond dependent coefficient, β is the ratio of distance from neutral axis to extreme tension fiber to distance from neutral axis to center of tensile reinforcement, d_c is the thickness of concrete cover measured from extreme tension fiber to center of bar (mm), and s is the longitudinal FRP bar spacing (mm).

It is worth mentioning that ACI 440.1R (2006) was using Eq. (1) for determining the crack width at service load. The ACI 440.1R (2015) replaced this equation with an indirect measure to control the crack width through the maximum spacing between the reinforcing bars (s_{max}) as shown in Eq. (2). The rationale of this indirect approach is described by Ospina and Bakis (2007). This approach, however, still includes the kb value. Both ACI 440.1R (2006) and (2015) state that for the case where kb is not known from experimental data, a conservative value of 1.4 should be used (excluding smooth bars and grids). In addition, ACI 440.1R (2015) cites the CSA S806 (2012) test method as appropriate measure to determine the kb values experimentally using Eq. (1) as conducted herein.

[3] $$s_{\max} = 1.15\frac{E_f\, w_{cr}}{f_f\, k_b} - 2.5C_c \le 0.92\frac{E_f\, w_{cr}}{f_f\, k_b}$$

Figure 8 introduces a comparison with the predicted crack widths for the BFRP bars using the available equations of ACI 440 (2006) and CSA S6 (2014). Since ACI 440.1R (2006) and (2015) guides in absence of experimental data proposes a conservative value of k_b = 1.4 and CSA S6 (2014) proposes k_b = 0.8 for sand-coated FRP bars, k_b values of 1.4, and 0.8 were used for ACI 440.1R (2006) and CSA S6 (2014), respectively. The comparisons in Figure 8 indicate that ACI 440 (2006) overestimates the crack widths for beams reinforced with BFRP bars. While CSA S6 (2014) yielded reasonable yet conservative crack width predictions.

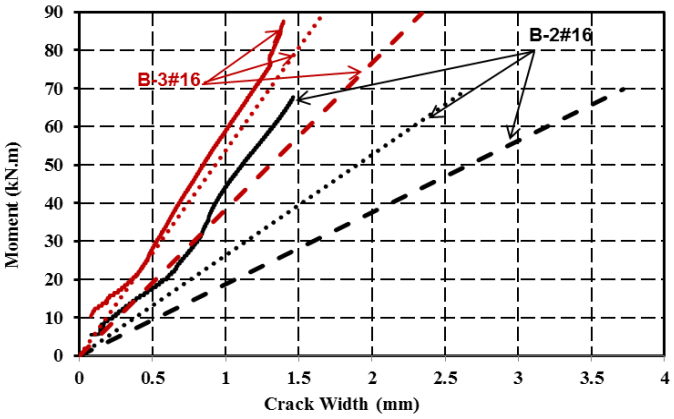

Figure 8: Measured and predicted crack widths for beams B-2#16 and B-3#16

4. CONCLUSIONS

Based on the test results and the discussions presented herein, the following conclusions were drawn:

Both the ACI 440.1R (2015) and CSA S806 (2012) provide reasonable predictions for the flexural capacity of FRP-RC beams (BFRP and GFRP). The average experimental-to-predicted ultimate capacities were 1.06±0.08 and 0.94±0.07 for ACI 440.1R (2015) and CSA S806 (2012), respectively.

Beams with similar axial stiffness, (B-2#16 and G-2#16) (B-3#16, G-3#16 and S-2#10M), have approximately similar reinforcement strains and deflection responses, regardless the reinforcement type or surface configuration.

The average k_b was 0.85 for ribbed BFRP bars which is lower than the current recommendations for deformed FRP bars by the Canadian Highway Bridge Design Code, CHBDC CSA S6 (2014).

ACKNOWLEDGMENTS

The authors wish to acknowledge the financial support of the Natural Sciences and Engineering Research Council of Canada (NSERC), the Canada Research Chair in Advanced Composite Materials for Civil Engineering, and the Fonds québécois de la recherche – Nature et Technologies - (FQRNT) of Quebec.

REFERENCES

ACI Committee 440. 2006. Guide for the Design and Construction of Concrete Reinforced with FRP Bars (ACI 440.1R-06). American Concrete Institute, Farmington Hills, Mich.

ACI Committee 440. 2012. Guide Test Methods for Fiber-Reinforced Polymers (FRPs) for Reinforcing or Strengthening Concrete Structures (ACI 440.3R-12), American Concrete Institute, Farmington Hills, USA.

ASTM D7205. (2011). "Standard Test Method for Tensile Properties of Fiber-Reinforced Polymer Matrix Composite Bars." American Society for Testing and Materials, Conshohocken, USA.

Bischoff, P., Gross, S., and Ospina, C. (2009). The Story behind Proposed Changes to the ACI 440 Deflection Requirements for FRP-Reinforced Concrete. ACI Special Publication, SP-264, 53–76.

Boyle, H.C. and Karbhari, V.M. 1994. Investigation of Bond Behavior between Glass Fiber Composite Reinforcements and Concrete. Journal of Polymer-Plastics Technology and Engineering, 33(6): 733-753.

Canadian Standard Association (CSA), 2014. Canadian Highway Bridge Design Code (CAN/CSA S6-14). Rexdale, ON, Canada.

Canadian Standard Association (CSA). 2010. Specification for Fibre-Reinforced Polymers (CAN/CSA S807-10). Rexdale, ON, Canada.

Canadian Standard Association (CSA). 2012. Design and Construction of Building Structures with Fibre Reinforced Polymers (CAN/CSA S806-12). Rexdale, ON, Canada.

El-Nemr, A., Ahmed, E., and Benmokrane, B. 2011. Instantaneous Deflection of Slender Concrete Beams Reinforced with GFRP Bars. 2nd International Engineering Mechanics and Materials Specialty Conference (CSCE), Ottawa, Ontario, June 14-17, (CD-ROM), 10 p.

ISIS Manual No 3. (2007). "Reinforcing Concrete Structures with Fibre-Reinforced Polymers." ISIS Canada Research Network, University of Manitoba, Winnipeg, MB.

Mota, C., Alminar, S., and Svecova, D. 2006. Critical Review of Deflection Formulas for FRP-RC Members. ASCE Journal of Composites for Construction, 3(10): 183-194.

Ospina, C.E., and Bakis, C.E. (2007). "Indirect Crack Control of Concrete Beams and One-Way Slabs Reinforced with FRP Bars," Proc. 8th Intl. Symp. on Fiber Reinforced Polymer Reinforcement for Concrete Structures, FRPRCS-8, T. C. Triantafillou, Ed., University of Patras, CD ROM, Paper 11-24, 9 pp. ISBN 978-960-89691-0-0.